body size — may be matched by the complexity of their social relationships.

**Richard C. Connor*, Michael R. Heithaus†, Lynne M. Barre‡**

**Biology Department, University of Massachusetts, Dartmouth, North Dartmouth, Massachusetts 02747, USA*
*e-mail: rconnor@umassd.edu*
*†Biology Department, Simon Fraser University, Burnaby, British Columbia, V5A 1S6, Canada*
*‡Biology Department, Georgetown University, Washington, DC 20057, USA*

1. Boehm, C. in *Coalitions and Alliances in Humans and Other Animals* (eds Harcourt, A. H. & de Waal, F. B. M.) 137–173 (Oxford Univ. Press, 1992).
2. Falger, V. S. E. in *Coalitions and Alliances in Humans and Other Animals* (eds Harcourt, A. H. & de Waal, F. B. M.) 323–348 (Oxford Univ. Press, 1992).
3. Connor, R. C., Smolker, R. A. & Richards, A. F. in *Coalitions and Alliances in Humans and Other Animals* (eds Harcourt, A. H. & deWaal, F. B. M.) 415–443 (Oxford Univ. Press, 1992).
4. Connor, R. C., Smolker, R. A. & Richards, A. F. *Proc. Natl Acad. Sci. USA* **89,** 987–990 (1992).
5. Connor, R. C. *et al. Behaviour* **133,** 37–69 (1996).
6. Wells, R. S. in *Dolphin Societies* (eds Pryor, K. & Norris, K. S.) 199–225 (Univ. California Press, Berkeley, 1991).
7. Connor, R. C. *et al.* in *Cetacean Societies: Field Studies of Whales and Dolphins* (eds Mann, J., Connor, R. C., Tyack, P. L. & Whitehead, H.) (Chicago Univ. Press, in the press).
8. Smolker, R. A. *et al. Behaviour* **123,** 38–69 (1992).
9. Nöe, R. *Anim. Behav.* **47,** 211–213 (1994).
10. Harcourt, A. H. in *Coalitions and Alliances in Humans and Other Animals* (eds Harcourt, A. H. & de Waal, F. B. M.) 445–471 (Oxford Univ. Press, 1992).
11. Cords, M. in *Machiavellian Intelligence* Vol. II, *Extensions and Evaluations* (eds Whiten, A. & Byrne, R. W.) 24–49 (Cambridge Univ. Press, 1997).
12. Barton, R. A. & Dunbar, R. I .M. in *Machiavellian Intelligence* Vol. II, *Extensions and Evaluations* (eds Whiten, A. & Byrne, R. W.) 240–263 (Cambridge Univ. Press, 1997).

# Anterior sphenoid in modern humans

Lieberman has proposed[1] that reduced midfacial projection (MFP), in which most of the face lies beneath the neurocranium, is a major unique, derived character of anatomically modern *Homo sapiens*, and that this reduction is largely a consequence of reduced anterior sphenoid length (ASL). Lieberman's conclusions were based on comparisons of a small sample of archaic *Homo* crania with those of Holocene and Pleistocene anatomically modern *H. sapiens*. We have made new measurements of ASL and MFP, and find that ASL was incorrectly estimated in those archaic fossil crania in which these landmarks are unambiguously preserved. It turns out that the anterior sphenoid in modern humans is no shorter than in archaic *Homo*.

The new measurements were taken from better-quality radiographs and computed tomography scans[2,3] and from the original specimens of Gibraltar 1 and Broken Hill (courtesy of C. Stringer, T. Molleson and F. Zonneveld). ASL values in Holocene and Pleistocene modern humans are 19.9 mm (s.d. 2.0) and 20.0 mm (s.d. 1.8), respectively[1], not significantly different ($P > 0.05$, Scheffé's $F$) from those of archaic *Homo* (Gibraltar 1, 17.2 mm; Monte Circeo, 16.9 mm; Broken Hill, 17.2 mm). Figure 1a confirms that reduced MFP in anatomically modern humans is not associated with a shorter ASL.

To assess the spatial relationships of ASL and MFP in relative terms, we did a geometric morphometric analysis comparing Holocene modern human crania with the three archaic *Homo* fossils (Fig. 1b,c). The transformation grid indicates that, relative to the size of the landmark configuration, MFP is shortened and ASL is lengthened in Holocene *H. sapiens*. The factors underlying these changes may include facial reduction, increased basicranial flexion, and expansion of the temporal lobes in the middle cranial fossae. The comparison also suggests that the pharyngeal area between the palate and the foramen magnum is anteroposteriorly constricted in Holocene modern humans, as was inferred by Lieberman[1], but that this is unrelated to ASL.

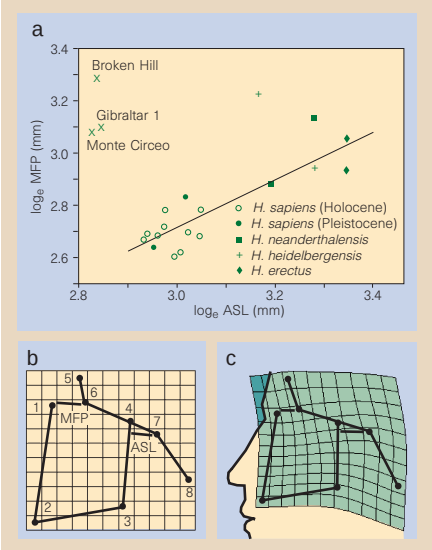


**Figure 1** Analysis of measurements. a, Plot of ASL and MFP (after Fig. 3a of ref. 1), with new measurements of Broken Hill, Gibraltar 1 and Monte Circeo. MFP is the distance from nasion to foramen caecum perpendicular to the posterior maxillary plane. ASL is the minimum distance from sella to the posterior maxillary plane. b, c, Geometric morphometric comparison of eight facial, neurocranial and basicranial landmarks from 28 combined-sex Holocene *H. sapiens* skulls (Indian subcontinent), Monte Circeo, Gibraltar 1 and Broken Hill. Principal components analysis of tangent coordinates following generalized Procrustes analysis yields 12 non-zero eigenvectors[4]. Only principal component I (PC I; 37% total shape variance) separates fossil from extant specimens. The shapes represent means for the fossils (b) and Holocene *H. sapiens* (c), both on PC I and each rescaled to their respective mean size. A cartesian transformation grid (thin plate spline[5]) from fossil to extant means is superimposed. Numbers: 1, nasion; 2, prosthion; 3, maxillary tuberosity; 4, laterally projected average intersection between greater wings and planum sphenoideum; 5, anteriormost point of cranial cavity; 6, foramen caecum; 7, sella; 8, basion (estimated in Neanderthals); 3 to 4, posterior maxillary plane.

We conclude that, although ASL is intraspecifically correlated with MFP in modern humans and chimpanzees[1], it does not account for the unique form of the modern human cranium. Our analysis highlights the need for research that integrates comparative morphometric analyses with developmental studies of cranial growth in human and non-human primates.

**Fred Spoor*, Paul O'Higgins*, Christopher Dean*, Daniel E. Lieberman†**

**Department of Anatomy and Developmental Biology, University College London, 21 University Street, London WC1E 6JJ, UK*
*e-mail: f.spoor@ucl.ac.uk*
*†Department of Anthropology, George Washington University, Washington, DC 20052, USA*
*e-mail: danlieb@gwu.edu*

1. Lieberman, D. *Nature* **393,** 158–162 (1998).
2. Sergi, S. in *The Circeo 1 Neanderthal Skull: Studies and Documentation* (eds Piperno, M. & Scichilone, G.) 23–173 (Istituto Poligrafico e Zecce dello Stato, Rome, 1991).
3. Silipo, P. *et al.* in *The Circeo 1 Neanderthal Skull: Studies and Documentation* (eds Piperno, M. & Scichilone, G.) 513–538 (Istituto Poligrafico e Zecce dello Stato, Rome, 1991).
4. Dryden, I. L. & Mardia, K. V. *Sankya A* **55,** 460–480 (1993).
5. Bookstein, F. L. *IEEE Trans. Patt. Anal. Mach. Intell.* **11,** 567–585 (1989).

# Iodine oxide in the marine boundary layer

A striking example of the influence of halogen chemistry on tropospheric ozone levels is the episodic destruction of boundary-layer ozone during the Arctic sunrise by reactive halogen species[1,2]. We detected iodine oxide in the boundary layer at Mace Head, Ireland (53°20′ N, 9°54′ W) during May 1997, which indicates that iodine chemistry is occurring in the troposphere.

Reactive halogen species in the atmosphere act as catalysts in several photochemical reaction cycles that are closely linked with ozone[3]. Iodine atoms react preferentially with ozone, forming iodine oxide, IO. IO can react with itself or with the halogen oxides BrO and ClO to produce $O_2$ and halogen atoms. If these react with ozone, a catalytic mechanism destroys two ozone molecules per cycle. The reaction of IO with $HO_2$ forms HOI, which is rapidly photolysed into I and OH. This catalytic cycle also effectively destroys ozone.

The measurement of IO in the boundary layer has so far been unsuccessful. The upper limit of the mixing ratios, determined as 0.5–0.9 part per trillion (p.p.t.)[3,4], agreed with model predictions[5–9]. We measured the concentrations of $O_3$, $NO_2$, $SO_2$, HCHO, HONO, BrO, ClO and IO by using long-path differential optical absorption spectroscopy (LP-DOAS)[10] during the

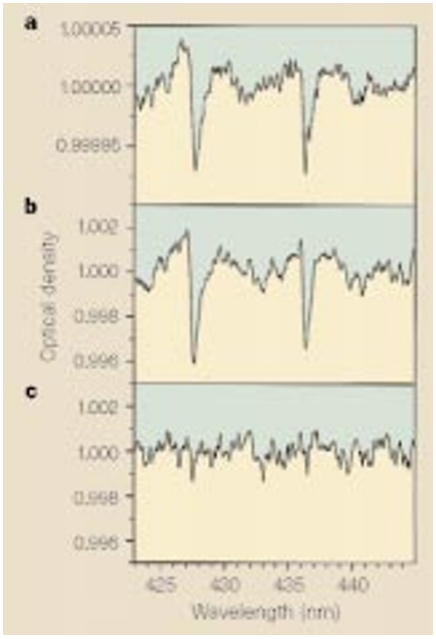


**Figure 1** Spectra. **a**, IO reference spectrum measured in the laboratory. **b**, Atmospheric absorption spectrum measured with DOAS[10] at a spectral resolution of 0.27 nm, after analysis. A fitting procedure scaled and subtracted the absorption of water (at 441–445 nm) and $NO_2$ which was below the detection limit. IO absorption bands are visible and agree in spectral position with the absorption cross-section[12] used to determine the mixing ratio of 6.6 ± 0.5 p.p.t. **c**, Residual spectral structure of the analysis, which determines the quality of the measurement.

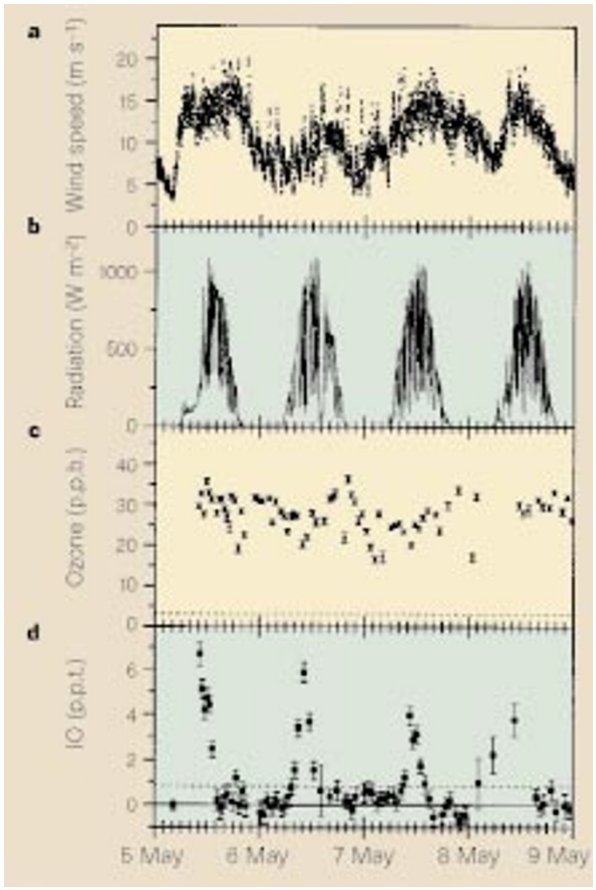


**Figure 2** IO and ozone measurements at Mace Head. Iodine levels were influenced by: **a**, wind speed; and **b**, global radiation. Mixing ratios and 1$\sigma$ errors of: **c**, ozone; and **d**, IO. Broken lines in **c** and **d** indicate the detection limit, defined as the average of twice the 1$\sigma$ errors in this period. Trace gases were below their respective detection limits of 1.7 p.p.t. BrO, 34 p.p.t. ClO, 70 p.p.t. $NO_2$, 170 p.p.t. HONO, 0.8 p.p.b. $SO_2$ and 0.4 p.p.b. HCHO. In the rest of the campaign, ozone varied between 15 and 50 p.p.b. Maxima of 4 p.p.b. $NO_2$ and up to 6 p.p.b. $SO_2$ were observed in polluted air masses.

HALOTROP/ACSOE field campaign at the atmospheric research station in Mace Head from 21 April to 30 May 1997. DOAS identifies and quantifies trace gases by their specific narrow-band (less than 5 nm) optical absorption structure in the open atmosphere, separating trace gas absorptions from broad-band molecule and aerosol extinction processes. A measured atmospheric spectrum after analysis is compared with a reference spectrum of IO in Fig. 1. The characteristic absorption bands of IO at 427.6 nm and 436.4 nm are both visible.

During 5–8 May 1997, IO concentrations increased above the detection limit of 0.9 p.p.t. The diurnal variation of IO follows solar radiation (Fig. 2). The ozone concentration during this period was about 30 ± 10 parts per billion (p.p.b.). The wind speed (Fig. 2) was higher than during the rest of the campaign. The wind was from the north, resulting in very clean air from the ocean. The correlation of IO concentrations with solar radiation indicates that iodine is produced by the photolysis of precursor species. Wind direction and preliminary trajectory analysis indicate that these species come from the ocean or the nearby shore. As there were increased concentrations of the short-lived iodinated hydrocarbons $CH_2I_2$ and $CH_2BrI$ (ref. 11), they were the most likely precursors.

We used a photochemical box model (see Supplementary Information) to estimate the magnitude of the different ozone-loss processes for 6 p.p.t. IO at noon. A loss of 0.06 p.p.b. ozone per hour is calculated for the IO self-reaction cycle. Assuming an upper limit to the mixing ratio of 1 p.p.t. for BrO and ClO, the crossreactions with IO would destroy less than 0.03 and 0.01 p.p.b. per hour, respectively. From the model, we calculated that there was about 6 p.p.t. of $HO_2$, leading to an effective ozone destruction of 0.27 p.p.b. per hour by the HOI cycle. In the presence of IO, the modelled $HO_2$ concentration decreases from roughly 8 to 6 p.p.t. owing to the reaction $HO_2 + IO$. The ratio of $[NO_2]/[NO]$ increases by about 30% as a result of the reaction NO + IO. At constant $NO_x$ (comprising NO and $NO_2$) levels of 70 p.p.t., both effects slow down photolytic ozone production by 0.06 p.p.b. per hour. A larger reduction of $O_3$ production is expected for higher $NO_x$ concentrations, up to a maximum of 0.15 p.p.b. per hour at 0.5 p.p.b. $NO_x$ (see Supplementary Information).

The estimated total ozone loss of 0.39 p.p.b. per hour is less than the observed variability of the $O_3$ concentrations of about 10 p.p.b. but has to be compared with the removal rate by dry deposition of around 0.1 p.p.b. per hour over the ocean and 1 p.p.b. per hour over land. Gas-phase reactions, such as photolysis to form OH radicals, destroy about 0.2 p.p.b. per hour of $O_3$ at noon. A mixing ratio of 6 p.p.t. IO can therefore increase the removal rate of ozone by about 70% over the ocean and 10% over land.

Our measurements show that IO, although recorded only over four days, exceeds the predicted tropospheric concentrations[5–9]. At levels of 6 p.p.t., IO can have a substantial influence on boundary-layer photochemistry. From our results and other data[11], we predict that IO should be present in clean air on coasts populated by macroalgae. Further investigation should establish the conditions that give rise to IO and the frequency of concentration increases.

**Björn Alicke, Kai Hebestreit, Jochen Stutz, Ulrich Platt**

*Institut für Umweltphysik, University of Heidelberg, INF 366, D-69120 Heidelberg, Germany*
*e-mail: stu@uphys1.uphys.uni-heidelberg.de*

1. Bottenheim, J. W. *et al. J. Geophys. Res.* **95,** 18555–18568 (1990).
2. Hausmann, M. & Platt, U. *J. Geophys. Res.* **99,** 399–413 (1994).
3. Wayne, R. P. *et al. Atmos. Environ.* **29,** 2675–2884 (1995).
4. Tuckermann, M. *et al. Tellus* **49B,** 533–555 (1997).
5. Chameides, W. L. & Davis, D. D. *J. Geophys. Res.* **85,** 7383–7398 (1980).
6. Jenkin, M. E. *AEA Environment and Energy Report AEA-EE-0405,* (AEA, 1992).
7. Solomon, S., Garcia, R. R. & Ravishankara, A. R. *J. Geophys. Res.* **99,** 20491–20499 (1994).
8. Sander, R. & Crutzen, P. J. *J. Geophys. Res.* **101,** 9121–9138 (1996).
9. Davis, D. *et al. J. Geophys. Res.* **101,** 2135–2147 (1996).
10. Platt, U. *Chem. Anal. Ser.* **127,** 27–83 (1994).
11. Carpenter, L. J. *et al. J. Geophys. Res.* (in the press).
12. Laszlo, B., Kurylo, M. J. & Huie, R. E. *J. Phys. Chem.* **99,** 11701–11707 (1995).

**Supplementary information** is available on *Nature*'s World-Wide Web site (http://www.nature.com) or as paper copy from the London editorial office of *Nature*.